In Situ Energy Dispersive X-ray Diffraction Study of $LiNi_{0.8}Co_{0.2}O_2$ Cathode Material for Lithium Batteries

F. Ronci, B. Scrosati,* V. Rossi Albertini, and P. Perfetti

Dipartimento di Chimica—Universita' "La Sapienza", P.le Aldo Moro 5, 00148, Roma, and Istituto di Struttura della Materia—CNR, Via del fosso del Cavaliere 100, 00133, Roma

Received: July 12, 2000; In Final Form: November 2, 2000

The investigation of structural changes of intercalation materials during cycling is of primary importance to understand the factors that limit their cyclability. In particular in-situ measurements, allowing the simultaneous acquisition of structural and electrochemical data, consent to directly correlate the cycling performance of the material under test to its structure evolution and vice versa.The energy dispersive X-ray diffraction (EDXD) technique has been applied to the study of the structural evolution of $LiNi_{0.8}Co_{0.2}O_2$ during several charge−discharge cycles performed with increasing anodic limits. This way of monitoring the effect of Li ions intercalation−deintercalation process on the host materials lattice parameters proved to be a valid alternative to the traditional angle dispersive X-ray diffraction (ADXD) method, solving some of its problems, first of all the question of the X-ray absorption.The results described in this paper confirm what reported in previous literature works based on in-situ ADXD and deepen the study of the $LiNi_{0.8}Co_{0.2}O_2$ structural changes, with large oversampling and good statistical accuracy, extending the investigation to the first 7 cycles with increased anodic limits approaching full delithiation.

Introduction

The X-ray diffraction has always been the main technique to perform investigations on powder samples.[1] However, a battery is a complex object and diffraction measurements cannot be carried out in a simple way like in the case of homogeneous samples contained in a sample holder expressly conceived for them. Both the transmission[2] and the reflection geometries[3,4] have been proposed for in-situ diffraction measurements and for both cases the cell container design has always been a very important factor. In fact, even simplifying the design of the battery as much as possible and arranging its components so that the electrode is directly exposed to the incident X-ray beam, the electrochemical requirements force to preserve a complicated geometry from the diffraction point of view.

In the transmission geometry, the cell must be very thin in all its components because the X-ray beam must pass through it with an acceptable intensity loss. Moreover, spurious peaks produced by the counter electrode and/or from the container itself are superposed to the sample diffraction pattern.

In the reflection geometry case, the cell must have very transparent windows, usually a thin beryllium foil, due to the high absorbance at low angles and, in most cases, the diffraction is carried out on the back electrode surface in order to avoid the electrolyte absorbance.[5]

For these reasons, all the reported methods require the use of cell containers having specific design or complicated mounting procedures, with the use of fragile and expensive parts (i.e., beryllium windows). Furthermore, the time needed for the cell construction starting from the electrode powder is often quite long.

We propose an alternative solution based on energy dispersive X-ray diffraction, EDXD to overcome some of these problems, which allowed the utilization of a very simple plastic cell container of a general design, not specifically designed for this purpose. Furthermore, the simplicity and steadiness of the EDXD instrumental setup enables us to perform long lasting acquisitions, so that a sequence of several cycles can be sampled in real time without any stability problem.

This method consists of irradiating the sample by a non-monochromatized X-ray beam, keeping the scattering angle unchanged.[6−7] In this case, the diffraction pattern is collected through the measurement of the energy spectrum of a polychromatic X-ray radiation scattered by a sample. From the detection point of view, EDXD makes use of the same instruments as the ordinary X-ray fluorescence spectroscopy. The difference is that the spectrum acquired in this way contains, besides the fluorescence lines (if any) of the irradiated sample, also its diffraction pattern: Bragg peaks, if the sample is crystalline, or much thicker hunch, if it is microscopically disordered like in the case of liquids and amorphous solids.

After a rescale of the energy axes, the normalization (to the incident intensity, the polarization and the X-ray absorption) and the background subtraction, the energy spectrum coincides with the ordinary diffractogram of the sample. The equivalence between EDXD and the traditional angular dispersive (ADXD) diffraction on powders is due to the fact that the intensity diffracted by a sample is a function of the momentum transfer q from the X-rays to the sample atoms. Since it depends both on the scattering angle 2ϑ and on the energy E of X-rays used for diffracting, two ways are possible to scan q, ADXD (E fixed, ϑ variable) and EDXD (ϑ fixed, E variable)

The advantages of EDXD are that no movement is needed during the data collection, which simplifies the measurement and the calculation of the quantities involved in the scattering process. Furthermore, the energy of the primary beam is higher, so that the X-ray absorption is strongly reduced. The main drawback is a certain loss of resolution in the diffractograms.[7]

* Author to whom correspondence should be addressed. E-mail: scrosati@uniroma1.it.

10.1021/jp0024827 CCC: $20.00
Published on Web 01/10/2001

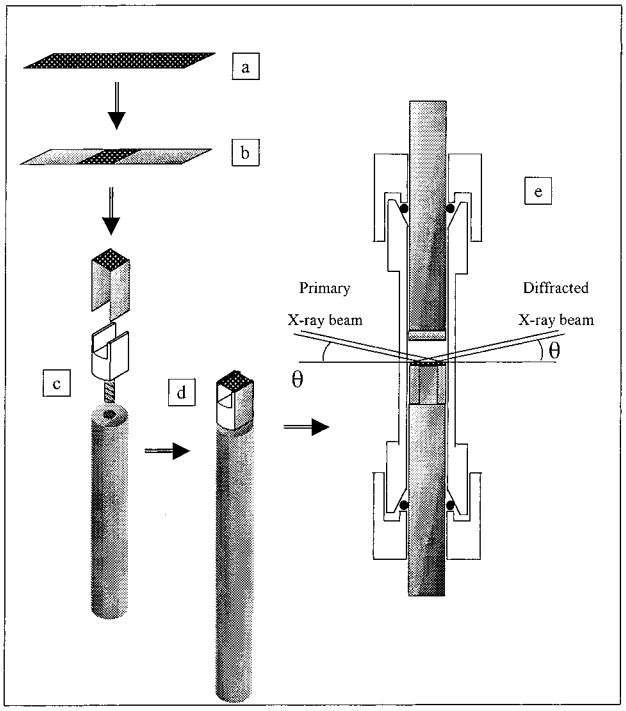

Figure 1. Schematic view of the experimental cell and of the method used to assemble it. (a) original membrane after deposition on an aluminum foil; (b) final aspect of the membrane after removing its external parts; (c) interposition of a plastic spacer to avoid the scattering from the steel cylinder; (d) sketch of the electrode after mounting; (e) section of the cell as arranged during the X-ray diffraction measurements.

In this work, the EDXD has been used to investigate the $LiNi_{0.8}Co_{0.2}O_2$ electrodic material. Since many Bragg peaks of it could be simultaneously observed, a very precise determination of the lattice parameters has been possible despite a slight broadening of each peak.[8]

Experimental Section

The Test Cell. The test cell used for this EDXD in-situ measurement is very simple, easy and fast to prepare even when starting from electrode powders. Indeed, this technique consents the use of metal lithium as the anode and of a standard liquid solution as the electrolyte, so that the study of the cathodic material can be performed under simple and reliable experimental conditions.

The container of the cell used in this work was a polymeric tube with 1 mm thick walls and 12 mm internal diameter. Two 304 stainless steel cylinders acting as current collectors were inserted inside it from the two opposite holes. The external parts of the cylinders were provided with two O-rings to guarantee the container sealing.

The first and largest part of the test cell preparation, partly illustrated in Figure 1, can be performed in open air, this allows us to avoid the difficulty of operating inside a glovebox.

The preparation started from the electrode membrane deposition on a thin aluminum foil. The membrane was composed by $LiNi_{0.8}Co_{0.2}O_2$ (Merck, active material), EPDM (Aldrich, binder) and Super P (MMM Carbon Belgium, electronic conductor) in the weight proportions 93:2:5. It was prepared using the standard doctor blade technique starting from a thoroughly mixed dispersion in toluene of the three components.

After solvent evaporation, a small piece of rectangular shape (Figure 1a), about 50 × 6 mm, was cut from the membrane and the two outmost parts were scraped in order to remove the deposited membrane from the aluminum leaving only a 6 × 6 mm central part covered (Figure 1b). This electrode membrane was placed on a specifically designed Teflon spacer, which separates the electrode from the cylinder in order to avoid the scattering from the steel (Figure 1c). The two opposite aluminum strips, folded laterally on the spacer, contacted the cylinder. In this way they guaranteed both the electronic contact and the mechanical tension of the electrode membrane itself (Figure 1d). The so-obtained working electrode was carefully put inside the polymeric container that was left open on the other side and then dried under vacuum at 120 °C for 24 h before being brought inside a Mbraun argon-filled glovebox having moisture and oxygen content below 1 ppm.

The final operations to be performed inside the glovebox were quite simple. A 12 mm diameter disk cut from a high purity lithium foil was attached on the second steel cylinder electrode. The container with the working electrode was then filled by a Merck battery grade lithium perchlorate, $LiClO_4$ 1M in ethylencarbonate−dimethyl carbonate, EC-DMC (1:1) liquid solution, without the use of any separator. The second electrode (counter) was pushed inside the container, allowing the excess electrolyte to exit, until it reached a distance from the working electrode of about 1 cm. Finally, the test cell was sealed and placed in the diffractometer center for the diffraction measurement (Figure 1d).

The Diffractometer. The energy dispersive diffractometer was constituted by an ordinary tungsten anode X-ray tube whose Bremmstrahlung (braking radiation) was used as primary beam. The fluorescence lines of the anode in the 9−11 keV region did not disturb the diffraction being completely absorbed by the cell walls and the electrolytic solution. The tube was supplied by a HV generator operating at 55.0 kV, so that the primary beam contained photons up to 55.0 keV.

The detector consisted of an ultrapure Ge single crystal that was able to distinguish the energy of each photon scattered in its direction. The energy spectrum was visualized on the computer screen by a multichannel analyzer connected to the detector amplifier.

In real time measurements of this kind, a series of spectra was collected while the cell was submitted to electrochemical cycling. Each spectrum of the series was acquired for a fixed time and automatically stored in the computer memory. Then, the system was reset and the acquisition of the subsequent spectrum begun.

The test cell was placed in the center of rotation of the diffractometer arms, which were inclined in the vertical plane by $\vartheta = 5.5°$ each with respect to the sample surface. In this way, a symmetric scattering geometry was obtained. It corresponded to a hybrid configuration, since it can be classified as transmission with respect to the cell walls and to the electrolytic solution, but reflection with respect to the sample and the Al current collector. For this reason an adaptation of the general EDXD instrumental equation[8] was required. However, it can be shown[9] that the signal produced by the sample only, i.e., in our case, the powder diffractogram of $LiNi_{0.8}Co_{0.2}O_2$, can be isolated from the total intensity observed at the detector, which contains many contributions. Taking into account that the X-ray absorption cuts the energy spectrum below 22 keV, the q-range scanned in these experimental conditions was about (2.1−5.3) $Å^{-1}$, which corresponds to an angular interval of (30°−81°) of an ADXD measurement where a Cu Kα wavelength is used. Many peaks (from the 101 to the 116) can be observed in this interval and the diffractograms fit provide very precise values for the lattice parameters.

In-Situ Measurements. The Li/$LiClO_4$ 1M EC-DMC (1:1)/$LiNi_{0.8}Co_{0.2}O_2$ test cell was cycled with a 22.8 μA current, corresponding to a C/72 rate if the total theoretical specific capacity (274 mAh/g) is considered. The cathodic limit was fixed at 3.1 V, while the anodic limit was 4.5 V during the first 3 cycles and incrementally increased to 4.6, 4.7, 4.8, 4.9 V in the subsequent 4 cycles.

The diffractograms were collected sequentially with a constant acquisition time of 1 h, corresponding to a theoretical composition variation during acquisition of $\Delta x = 0.014$ in $Li_xNi_{0.8}Co_{0.2}O_2$ and to a theoretical sampling of the lattice parameters of 72 points per charge (or discharge). In this way, both the electrochemical constraint (low concentration gradients) and the diffraction constraint (sufficient signal statistics) were fulfilled, together with a dense sampling of the lattice parameters during the charge and discharge processes. Dense sampling means that the duration of each spectrum collection is much shorter than the characteristic time of structural change of the powder. Otherwise, if this condition was not met, the diffractograms of the sequence would represent an average structure over the time interval of acquisition.

The observed spectra were normalized to the characteristic quantities of the measurement (intensity of the incident beam, X-ray absorption and polarization) and the other contributions to the scattering (plastic cell walls, electrolytic solution, Al foil) were subtracted according to the EDXD theory.[9] The a ($=b$) and c lattice parameters evolution upon cycling was obtained by fitting the previous normalized diffractograms using the PowderCell 2.1 nonlinear least-squares fitting software.

Results and Discussion

Figure 2 shows the series of diffractograms collected during the first 3 cycles. The patterns relative to the current inversion points (anodic and cathodic limits) are evidenced by using thicker lines. After normalization, all the patterns were fitted using the R$\bar{3}$m space group.[10]

Figure 3 reports the parameters evolution as a function of time together with the profile of the cell voltage, the calculated unit cell volume and the theoretical intercalation degree x in $Li_xNi_{0.8}Co_{0.2}O_2$, estimated assuming that the only reaction occurring was the intercalation/deintercalation process.

Many features are visible by examining these figures. During the first charge to 4.5 V the deintercalation process proceeds to the theoretical composition of about $Li_{0.05}Ni_{0.8}Co_{0.2}O_2$. The lattice parameters evolution confirms the expected behavior, i.e., a monotonic decrease of the a parameter and an almost linear increase of c up to $x = 0.35$. This is clearly visible in Figure 2 by noticing the progressive splitting of the overlapping 108 and 110 peaks. In fact, the former, being mostly dependent on c, moves to lower energies during charge, while the latter, depending only on a, moves to higher values. In this range, which corresponds to 3/4 of the theoretical specific capacity, the unit cell volume changes between 101 and 99 Å^3, with a percent variation of about 2%. Further deintercalation beyond $x < 0.35$ produces a drastic decrease in the c value, this greatly influencing the unit cell volume with a variation close to 4%, i.e., from 99 to 95 Å^3.

The trend of the c parameter, already reported for the parent $LiNiO_2$[11] and $LiCoO_2$[12] compounds, can be explained on the basis of the repulsion effect between adjacent (O−M−O) slabs, where M = Ni, Co, as described in Figure 4a which shows the structure of the fully lithiated $LiNi_{0.8}Co_{0.2}O_2$ compound. Initially the M ions are in the 3+ charge state, so the $(O-M-O)_n$ slab

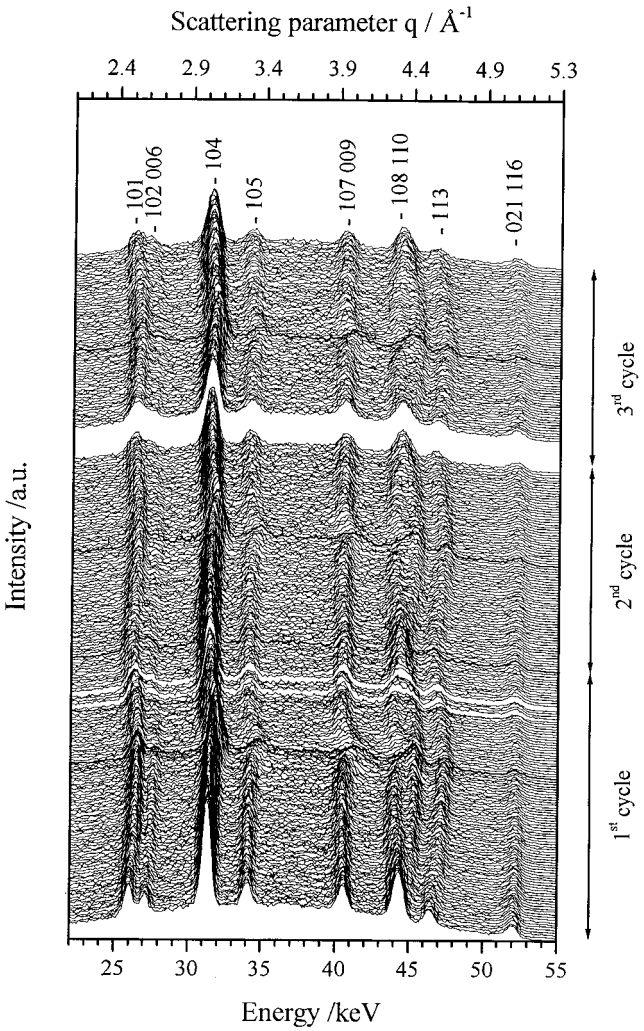

Figure 2. Sequence of diffraction spectra of the $Li_xNi_{0.8}Co_{0.2}O_2$ electrode material recorded during the first three charge (Li-deintercalation)−discharge (Li-intercalation) cycles performed maintaining the upper charge voltage limit at 4.5 V. The thicker profiles indicate the end of each charge or discharge. The Miller indexes reported correspond to the R$\bar{3}$m space group.

has a net charge of $n-$, which is balanced by the $n+$ charge of the lithium ion slab $(Li)_n$. As the charge process proceeds, the oxidation of the M ions from 3+ to 4+ and the concomitant deintercalation of lithium ions produces a decrease in the electrostatic attraction between the $(O-M-O)_n$ and the $(Li)_n$ adjacent slabs. Indeed, the deintercalation reaction can be regarded as a formal positive charge transfer from the $(Li)_n$ to the $(O-M-O)_n$ slab (concomitant Li^+ deintercalation and M^{3+} oxidation to M^{4+}), which reduces the slabs net charge respectively to $xn+$ and $xn-$, where x is the intercalation degree.

This phenomenon causes an initial increase in the c parameter, because of the diminished attraction between $(O-M-O)_n$ and $(Li)_n$ slabs. Proceeding with the deintercalation process, the $(O-M-O)_n$ slabs tend to become more and more neutral while the $(Li)_n$ slabs occupancy decreases. As a consequence, the repulsion between adjacent $(O-M-O)_n$ slabs is progressively reduced and, for low x values, a closer packing in the direction of the c parameter becomes possible.

The discharge process shows a specular trend in both the curves, but the values are not overlapping, due to the partial irreversibility of the first charge, which is a common phenomenon in layered intercalation compounds. The second and third

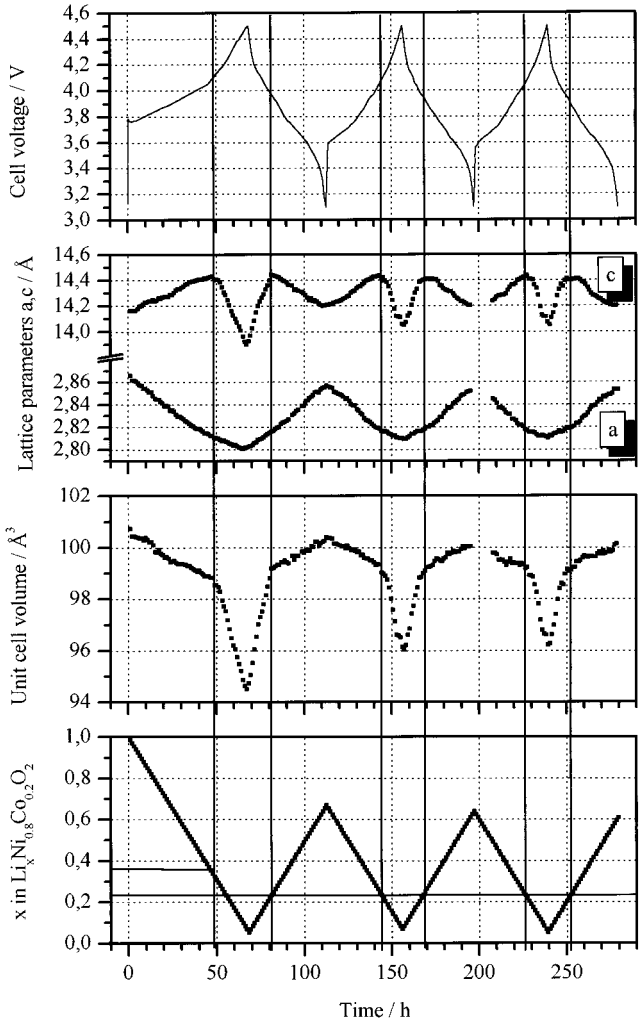

Figure 3. Time evolution of the cell voltage, lattice parameters, unit cell volume, and x level of $Li_xNi_{0.8}Co_{0.2}O_2$ measured during the three initial charge−discharge cycles.

cycles, performed under the same experimental conditions, show a similar trend, but in this case the reversibility of the electrochemical process is confirmed by the reversibility of the structural changes. It is worth noting that the inversion of the *c* curve takes place at a constant value of about $x = 0.25$, while in the first charge it occurs at about $x = 0.35$.

The *a* and the *c* trends related to the first and to the second charge processes are reported in Figure 5. The trends are reproducible and the second charge curve overlaps with the first, except for the initial and final parts. This suggests that two different irreversible phenomena occur during the first charge.

The values of the structural parameters at the beginning of the second charge ($a = 2.857$ Å and $c = 14.20$ Å) match the values found in the first charge curves when x is about 0.9. This suggests that the deintercalation of the first 0.1 equivalents is an irreversible process, most probably due to the a semiconductor−metal transition[13,14] that does not consent a full reintercalation process during the discharge process at normal current rates.

A second irreversible part is occurring at high cell voltage. This is probably due to the stress induced by the large variation in the unit cell volume and cannot be attributed to an electrolyte decomposition reaction because, should this be the case, no structural changes at all would have occurred, see below. The volume change, due to deintercalating beyond $x = 0.25$ could be viewed as one of the causes of the specific capacity loss of

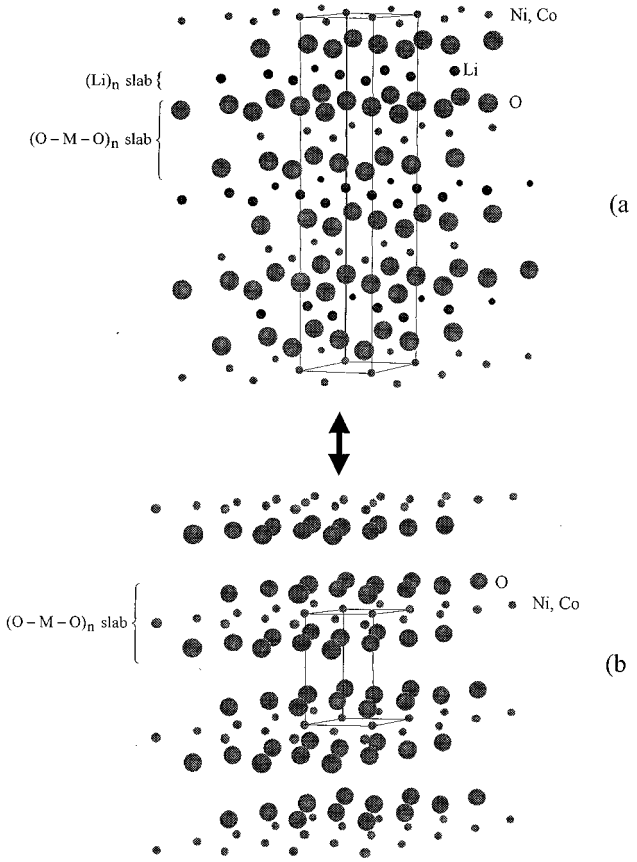

Figure 4. Schemes of the structures of the $LiNi_{0.8}Co_{0.2}O_2$ two phases, corresponding to the lithiated compound ($R\bar{3}m$, a) and to the same compound after total removal of Li ($P\bar{3}m1$, b).

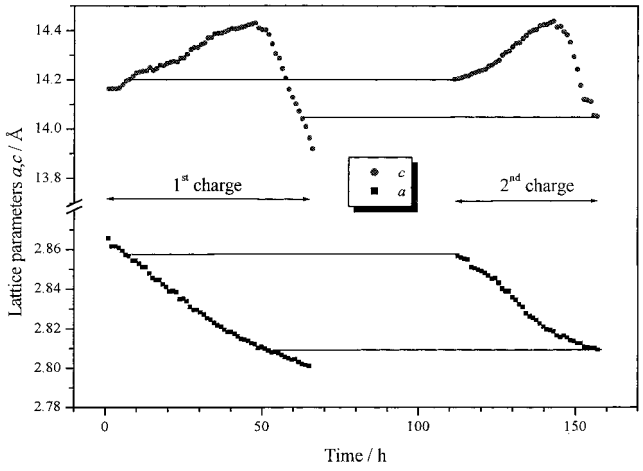

Figure 5. Comparison between the portions of the *a* and *c* parameter curves relative to the first and the second charge of $Li_xNi_{0.8}Co_{0.2}O_2$, to evidence the occurrence of irreversible effects.

$LiNi_{0.8}Co_{0.2}O_2$ when cycled at high voltage and/or at high current rates. In fact, as recently proposed by Uchida and co-workers to the $LiNiO_2$ case,[15] attempts of extending the charge process to high voltage result in breaking the cathode particles, with a consequent loss of electronic contact and thus, of overall capacity.

Figure 6 reports the second part of the diffractogram series, being relative to the interval between the fourth and seventh cycle, performed with anodic limits progressively increasing from 4.6 to 4.9 V. The most important feature visible in this series is the phase transition, i.e., from $R\bar{3}m$ (O3 type) to $P\bar{3}m1$ (O1 type), occurring at the end of the seventh cycle. The

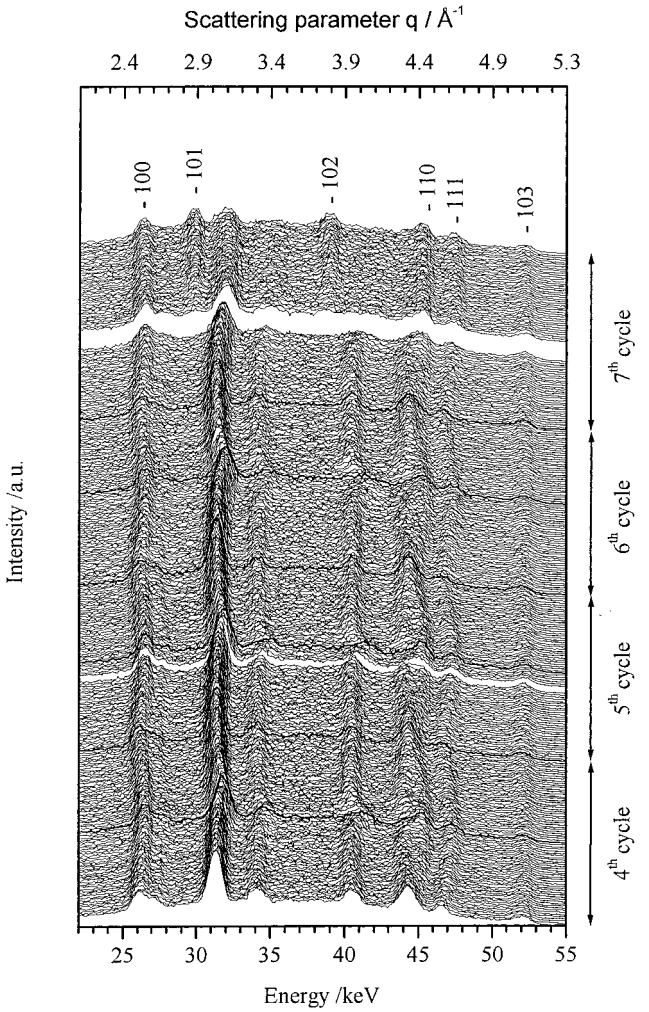

Figure 6. Sequence of diffraction spectra as in Figure 2, corresponding to the subsequent charge−discharge cycles (4th−7th) of the $Li_xNi_{0.8}Co_{0.2}O_2$ electrode material. At each cycle the anodic limit was increased from 4.5 V by steps of 0.1 V. During the last charge to 4.9 V, the onset of peaks denoting the appearance of a new phase ($P\bar{3}m1$) can be noticed. The Miller indexes reported correspond to this space group.

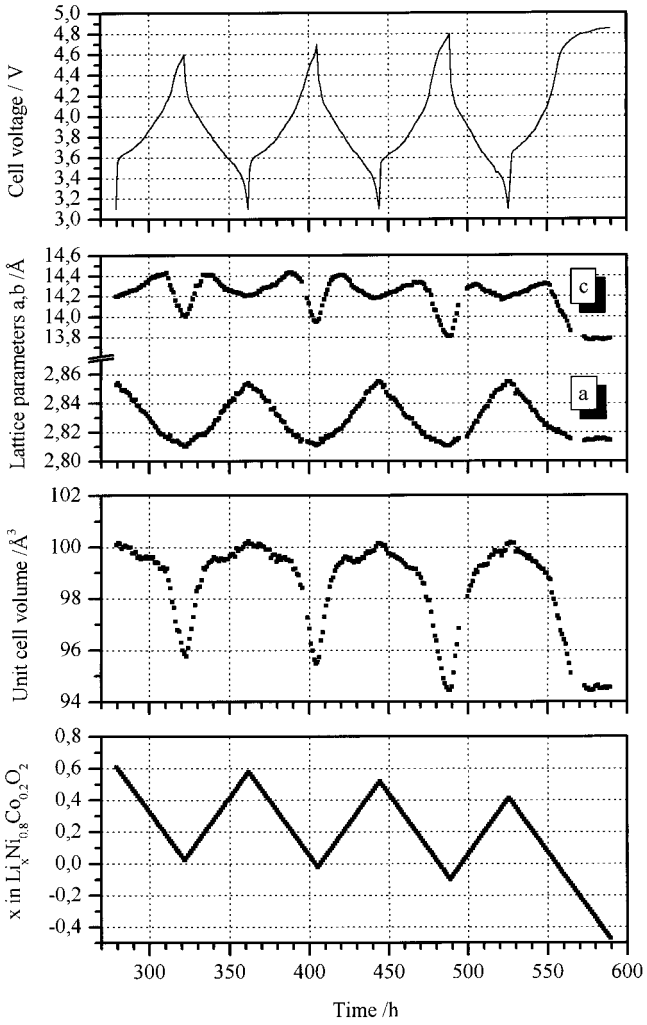

Figure 7. Time evolution of the cell voltage, lattice parameters, unit cell volume, and x level of $Li_xNi_{0.8}Co_{0.2}O_2$ measured during the 4th to the 7th charge−discharge cycles.

reflections reported in the figure are referred to the $P\bar{3}m1$ phase. This transition was already reported for $LiCoO_2$[16] and for $LiNiO_2$[17] upon fully delithiation and can be described as a change in the relative stacking of the $(O-M-O)_n$ slabs, see Figure 4b, which shows the structure of $Ni_{0.8}Co_{0.2}O_2$ after total lithium removal.

The results from the normalization and fitting of these spectra are reported in Figure 7. For the sake of continuity the value of the c parameter curve is multiplied by 3 in the case of the $P\bar{3}m1$ phase. As the anodic limit is increased to 4.6, 4.7, 4.8, and 4.9 V, this value, and consequently that of the unit cell volume, is more and more reduced, while the a curve does not show major changes in successive cycles. It is important noting that the theoretical intercalation degree x in $Li_xNi_{0.8}Co_{0.2}O_2$ appears to reach negative values, demonstrating the occurring of irreversible oxidative reactions as the anodic limit is increased. That is the reason the x value at which the inversion of the c curve takes place is different from 0.25 and becomes more and more negative. The above quoted irreversible process could be due to the structural stress already described and/or to the onset of an electrolyte decomposition reaction, clearly visible in the very final part of the cyclation, where the cell voltage reaches a plateau at about 4.88 V and the lattice parameters show a constant value of $a = 2.814$ Å and $c = 13.77$ Å.

Conclusions

The structural variation of the $Li_xNi_{0.8}Co_{0.2}O_2$ electrode material was studied in situ as a function of x during the first 7 cycles by means of the energy dispersive X-ray Diffraction. Thanks to this innovative technique it was possible to study the structural evolution of this material over the entire Li intercalation range, even approaching full delithiation, under simple and reliable experimental conditions, i.e., by using a lithium anode, a liquid electrolyte, and a simple cell container. The results suggest that the partial irreversibility of the first charge (Li deintercalation process) is due to two different phenomena occurring at the beginning and at the end of the charge process, respectively. The first is the irreversible deintercalation of the initial 0.1 Li equivalents, quite likely due to the poor electronic properties of $Li_xNi_{0.8}Co_{0.2}O_2$ for $x > 0.9$. The second is most probably due to the structural stress induced by deep Li deintercalation, i.e., for $x < 0.25$.

Extending the anodic voltage limit to higher values resulted in an even deeper deintercalation, which reflected into a more drastic reduction of the c parameter and, consequently, of the unit cell volume. Furthermore, as the cell voltage approached 4.9 V, the evidence of a phase transition from the $R\bar{3}m$ (O3 type) to the $P\bar{3}m1$ (O1 type) structure was found.

References and Notes

(1) Klug, H. P.; Alexander, L. E. *X-ray diffraction procedures*; John Wiley and sons: New York, London, 1st ed., 1902; 2nd ed., 1954; 3rd ed., 1974.

(2) Robinson, K. M.; O'Grady, W. E. *Rev. Sci. Instrum.* **1993**, *64* (4), 1061.

(3) Nahle′, A. H.; Walsh, F. C.; Brennan, C.; Roberts, K. J. *J. Appl. Crystallogr.* **1999**, *32*, 369.

(4) Mukerjee, S.; Thurston, T. R.; Jisrawi, N. M.; Yang, X. Q.; McBreen, J.; Daroux, M. L.; Xing, X. K. *J. Electrochem. Soc.* **1998**, *145* (2), 466.

(5) Richard, M. N.; Koetschau, I.; Dahn, J. R. *J. Electrochem. Soc.* **1997**, *144* (4), 554.

(6) Caminiti, R.; Rossi Albertini, V. *Int. Rev. Phys. Chem.* **1999**, *18*, 263.

(7) Ronci, F.; Scrosati, B.; Rossi Albertini, V.; Perfetti, P. *Electrochem. Solid State Lett.* **2000**, *3* (4), 174.

(8) Nishikawa, K.; Iijima, T. *Bull. Chem. Soc. Jpn.* **1984**, *57*, 1750.

(9) Ronci, F.; Scrosati, B.; Rossi Albertini, V.; Perfetti, P. *Chem. Mater.*, in press.

(10) Levi, E.; Levi, M. D.; Salitra, G.; Aurbach, D.; Oesten, R.; Heider, U.; Heider, L. *Solid State Ionics* **1999**, *126*, 97.

(11) Li, W.; Reimers, J. N.; Dahn, J. R. *Solid State Ionics* **1993**, *67*, 123.

(12) Ohzuku, T.; Ueda, A. *J. Electrochem. Soc.* **1994**, *141* (11), 2972.

(13) Molenda, J.; Stopklosa, A.; Bak, T. *Solid State Ionics* **1989**, *36*, 53.

(14) Croce, F.; Nobili, F.; Deptula, A.; Lada, W.; Tossici, R.; D′Epifanio, A.; Scrosati, B.; Marassi, R. *Electrochem. Commun.* **1999**, *1*, 605.

(15) Dokko, K.; Nishizawa, M.; Horikoshi, S.; Itoh, T.; Mohamedi, M.; Uchida, I. *Electrochem. Solid State Lett.* **2000**, *3* (3), 125.

(16) Amatucci, G. G.; Tarascon, J. M.; Klein, L. C. *J. Electrochem. Soc.* **1996**, *143* (3), 1114.

(17) Croguennec, L.; Pouillerie, C.; Delmas, C. *J. Electrochem. Soc.* **2000**, *147* (4), 1314.